Preference-based Assistance Map Learning with Robust Adaptive Oscillators

Shilei Li, Wulin Zou, Pu Duan and Ling Shi

***Abstract*—Recently, lower-limb exoskeletons have demonstrated the ability to enhance human mobility by reducing biological efforts with human-in-the-loop (HIL) optimization. However, this technology is confined to the laboratory, and it is difficult to generalize to daily applications where gaits are more complex and professional equipment is not accessible. To solve this issue, firstly, we present a robust adaptive oscillator (RAO) to synchronize the human-robot movement and extract gait features. Then, we use the Gaussian process regression (GPR) to map the subjects' preferred assistance parameters to gait features. Experiments show that the RAO has a faster convergence rate compared with the traditional adaptive oscillators. Meanwhile, the learning efficiency of the proposed method shows superiority compared with the HIL optimization. The effectiveness of the proposed method is validated by a hip exoskeleton at a speed of 5 km/h with 7 participants. Three muscles which include rectus femoris, tibialis anterior, and medial gastrocnemius are investigated in three conditions: user-preferred assistance (ASS), zero torque (ZT), and normal walking (NW). The results show that all muscles achieve an activity reduction in ASS mode compared with ZT or NW. Meanwhile, there is a statistically significant difference on medial gastrocnemius in ASS mode with respect to both ZT and NW ($-15.63 \pm 6.51\%$ and $-8.73 \pm 6.40\%$, respectively).**

***Index Terms*—robust adaptive oscillators, Gaussian process regression, muscle activities, hip exoskeleton.**

I. Introduction

Wearable robots have demonstrated the ability of enhancing walking economy for both healthy subjects [1]–[5] and patients [6], [7] with passive or active devices. Though the unpowered exoskeletons own less mass penalty, the powered devices can provide more flexible assistance and deliver much stronger strength [8], hence, are much more popular [1]–[3], [6]–[8]. Many devices have broken the "metabolic barrier" [1], [2], [4], [8] and demonstrate muscle activities reduction [3] in a laboratory environment. However, there is a research gap in transferring these technologies to daily applications.

One challenge of using these technologies in daily life is human-robot movement synchronization. In contrast to the designated speed walking on the treadmill in a laboratory, gaits are more agile and complex in a community, which brings difficulties to gait phase estimation. Traditionally, the gait phase can be obtained by interpolating two adjacent gait events, e.g., the heel strike or the maximum hip flexion moments by force sensors [1], [3] or inertial measurement units (IMUs) [2], [9]. However, this method requires extra sensors and may cause a considerable phase error when gaits switch between high and low speeds. Another solution is adaptive oscillators (AO) [10]–[14] which obtain a continuous gait phase based on gait-related periodical signals, such as joint angles [11], non-contact capacitive sensing [12], or foot-to-foot distance [13]. The flexibility of sensor requirements in AO can significantly simplify the design of the exoskeleton and hence it is favored by many researchers [10]–[14]. Nevertheless, this method possesses a trade-off between the algorithm stability and convergence rate and may cause a phase error when the input signals change from one frequency to another. The unsatisfactory gait phase may induce improper assistance, leading to discomfort and even gait instability. Therefore, it is necessary to improve the convergence rate of AO while maintaining its stability.

Another challenge is the individualized assistance map construction. Through evolution, our muscular, skeletal, and neural systems are well-suited to locomotion [15], [16]. We train our walking coordination strategy over a lifetime and keep a low energy expenditure when walking, which increases the difficulty of reducing biological efforts using external devices, such as powered exoskeletons. Previous strategies for biological effort reduction include simulations [17], biomechanical measurements [18], and mathematical models [19]. However, these approaches are difficult to generalize to different subjects due to individuals' physiological and neurological differences [20]–[22]. Parameter sweep [21]–[23] is a possible method to find the optimal assistance. However, it is time-consuming, especially when the parameter dimension is high. Recently, human-in-the-loop (HIL) optimization has emerged and attracted a lot of research effort since it is an automatically discovering, customizing, and continuously adapting strategy [1], [2], [24]. However, this approach not only requires indirect calorimetry equipment when walking but also is time-consuming (83 ± 14 min, 21.4 ± 1 min, 50 min in [1], [2], [24], respectively). More importantly, it ignores users' preferences and may induce discomfort and speed up fatigue [3].

To solve the aforementioned problems, we develop a robust adaptive oscillator (RAO) for the synchronization of humans and robots and employ the Gaussian process regression (GPR) for assistance map construction. AO was proposed by Righetti et al. [25] to synchronize with periodic or pseudo-periodic signals using the dynamic Hebbian learning rule. Then, it was

Manuscript submitted June 9, 2021. This work was supported by Shenzhen-Hong Kong Technology Cooperation Funding Scheme under Grant GHP-001-18SZ.

Shilei Li, Wulin Zou, and Ling Shi are with the Department of Electronic and Computer Engineering, The Hong Kong University of Science and Technology, Hong Kong, China (e-mail: slidk@connect.ust.hk, wzouab@connect.ust.hk, eesling@ust.hk).

Shilei Li, Wulin Zou, and Pu Duan are with Control Department, Xeno Dynamics, Co., Ltd, Shenzhen 518055, China (e-mail: lishilei@xeno.com, zouwulin@xeno.com, duanpu@xeno.com).

utilized for human-robot synchronization by extracting elbow motion features and compensating for elbow dynamics [10]. To enhance its capability, Ronsse et al. [26] coupled it with kernel-based filters for velocity and acceleration estimation, while Seo et al. [11] proposed a particularly-shaped adaptive oscillator (PSAO) to estimate the gait phase based on a single hip angle. Notably, AO employs a gradient-based method for phase estimation, thereby inevitably owning a phase lag when input signals are non-steady. To mitigate this problem, Zhang et al. [12] designed an extra phase reset and phase error learning block to identify the zero-phase point and compensate for the phase error, while Xue et al. [14] developed a dual-oscillator structure to alleviate the phase error. Though the above methods can improve AO's performance to some extent, they possess the drawbacks of requiring prior knowledge [11] or additional sensors [12], and their performances may be unsatisfactory with gait transition (e.g., switching from slow walking to rapid walking). In this paper, we use the zero-cross points of two hip angles to identify both the zero phase and gait frequency. Then, we utilize this information to correct the oscillator dynamics. The new oscillator is called the robust adaptive oscillator (RAO), which can align the zero phase automatically and has a faster convergence rate compared with AO.

Many bio-mechanical measurement-based strategies have been utilized to obtain assistance maps, such as parameter sweep [21]–[23] and HIL optimization [1], [2], [24]. However, to the best of our knowledge, preference-based assistance map construction has not been explored before. In this paper, we propose a Gaussian process regression-based (GPR) learning strategy, which explores the assistance profile based on users' proprioceptive feedback rather than biomechanical measurement. The purpose of this work is to investigate the feasibility of constructing assistance maps based on the user's preference. The proposed method has some advantages compared with the traditional HIL method. Firstly, it does not need indirect calorimetry equipment and is user-friendly. Users can explore different assistance profiles and evaluate their utilities through their proprioceptive feedback easily. It is worth mentioning that this process can be conducted in daily walking, hence is very convenient. Secondly, our method is more efficient than HIL optimization. One reason is that the HIL strategy may disturb the predictive forward model in our motor systems [27] since the user cannot predict the changes of the following control strategy. Hence, users need to spend more time adapting to the machine. Another reason is that signals from the calorimetry device are very noisy and have to be averaged within a few minutes, which hinders the fast convergence of HIL. Fortunately, these drawbacks can be avoided by the preference-based learning method since the assistance profile is adjusted based on the users' selection and is completely predictive. Moreover, users can evaluate their "preference score" in a few seconds. Hence, the learning efficiency of the proposed method should be higher. Thirdly and most importantly, the interaction comfort, as an important criterion of wearing experience, is ignored by HIL. However, it can be accessed by our proprioception system [28]–[30] naturally. Bertram [31] showed that humans prefer gaits with a lower metabolic expenditure. This indicates that users can 'feel' the biological efforts and try to select the most labor-saving walking strategy. Actually, preference-based learning can be regarded as a combination of multi-purpose optimization, which includes both interaction comfort and biological effort reduction. This combined objective should be more reasonable and practical than the single metabolism reduction criterion in a practical application. The contributions of this paper are summarized as follows:

1) A RAO is designed which can align the zero phase automatically and has a faster convergence rate compared with AO.
2) A preference-based learning strategy is utilized to construct assistance maps. The proposed method owns the advantages of not requiring additional equipment, efficient procedure, and interaction comfort.
3) The user-selected assistance profile is validated by investigating muscle activities at 5 km/h on the treadmill. The results reveal that the user-selected assistance can achieve a considerable muscle activity reduction compared with zero torque mode.

The remainder of this paper is organized as follows. In Section II, the approach overview is introduced, which includes the design of RAO, the exoskeleton torque controller, and the GPR. In Section III, some experiments are conducted to verify the effectiveness of the proposed methods. In Section IV, a conclusion is drawn.

II. Materials and Methods

A. Approach Overview

A hip exoskeleton prototype provided by Xeno Dynamics Co., Ltd is used. The control board is installed on the back of the device, which collects absolute joint angle and interactive torque data from sensors at the hip joints. Belts at the shoulders, waist, and thighs are employed to assure the force (or torque) transfer. The mass of the exoskeleton concentrates on the waist and its weight is 4.5 Kg. A diagram of the hip exoskeleton is shown in Fig. 1.

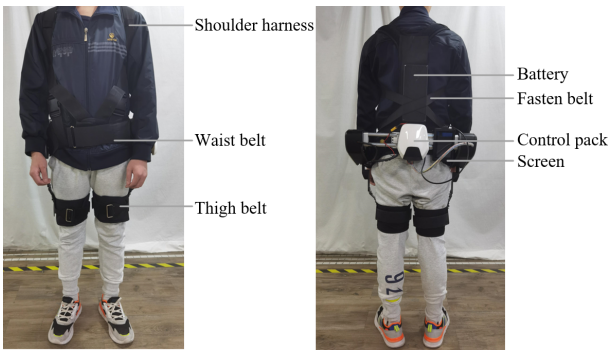

Fig. 1. Front and rear view of the hip exoskeleton. An elastic fasten belt is used to avoid the exoskeleton waist flip.

The overall control architecture is shown in Fig. 2. It is composed of three components. The first component is the gait perception module, where a RAO is deployed to obtain the gait cycle percentage c and extract the gait features g. The

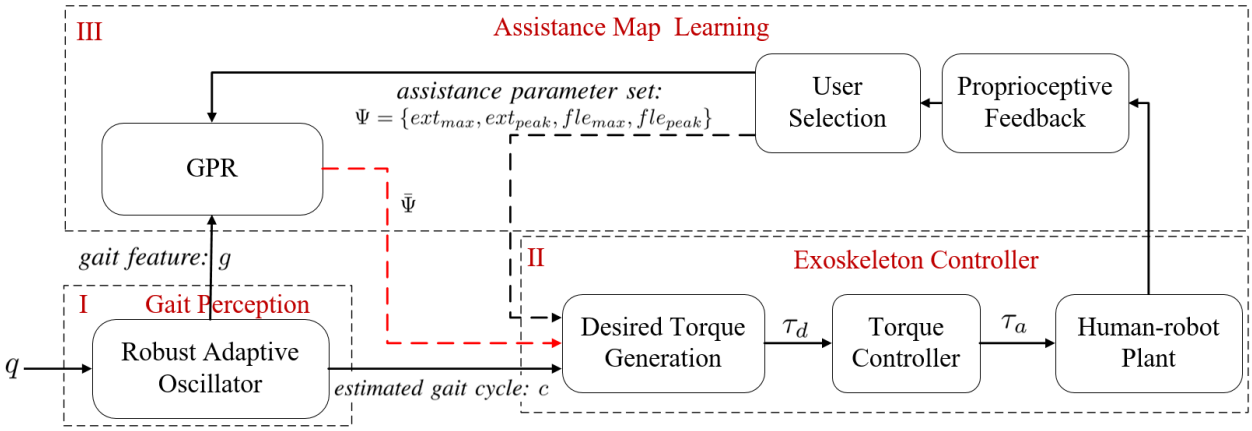

Fig. 2. Overview of the control architecture. First, gait is analyzed by a robust adaptive oscillator and its output is gait cycle c and gait feature g. Then, the desired torque is generated based on c and its shape is controlled by a human-machine interface. After that, the exoskeleton carries out the command and assists the subject. In this process, the user can adjust the assistance profile and submit their satisfied parameters based on their proprioceptive feedback. A Gaussian process regression (GPR) module is employed to imitate the user's preference and to map the gait features g to the users' preferred parameter set Ψ. After the learning procedure, the exoskeleton can automatically provide suitable assistance based on the user's gait feature without manipulating the human-robot interface.

input of this module is the difference between two hip angles $q = \theta_r - \theta_l$ where θ_r and θ_l are the right and left hip angle. As for the exoskeleton controller module, the desired torque is designed based on gait cycle percentage c and is controlled by parameter set $\Psi = \{ext_{max}, ext_{peak}, fle_{max}, fle_{peak}\}$. Then, a low-level torque controller is designed to track the desired torque profile. The final component is the assistance map learning module which includes a training session and a learning session. In the training session, users are required to walk at different speeds on a treadmill with different gait features (i.e., different gait amplitudes and frequencies). Then, they explore and submit their preferred assistance parameter set Ψ through a human-robot interface. The GPR predicts the user-preferred assistance profiles based on the historical data. The objective of this module is to minimize the difference between the human selected parameter set Ψ and the predicted parameter set $\bar{\Psi}$ based on the training set. After the learning procedure, the exoskeleton can automatically provide an individualized assistance profile when walking at different speeds.

B. Robust Adaptive Oscillators

In the conventional AO, a periodic (or quasi-periodic) signal q is estimated by a pool of sinusoidal curves with

$$\hat{q} = \sum_{i=0}^{K} \alpha_i sin(\phi_i) = \sum_{i=0}^{K} \alpha_i sin(iwt + \beta_i) \tag{1}$$

where K denotes the order of the harmonics, w is the fundamental frequency, α_i is the amplitude for i-th order harmonic, and β_i is the offset phase. Note that ϕ_0 is set to be $\pi/2$ so that α_0 is a bias term. The learning rule is shown as follows:

$$\begin{cases} \dot{\phi}_i(t) = iw(t) + v_\phi \frac{e(t)}{\sum_{i=0}^{K} \alpha_i(t)} \cos\phi_i(t) \\ \dot{\alpha}_i(t) = \eta e(t) \sin\phi_i(t) \\ \dot{w}(t) = v_w \frac{e(t)}{\sum_{i=0}^{K} \alpha_i(t)} \cos\phi_1(t) \end{cases} \tag{2}$$

with

$$e(t) = q(t) - \hat{q}(t)$$

where $q(t)$ is the input signal, $\hat{q}(t)$ is the estimated signal obtained by (1), $e(t)$ is the tracking error, and v_ϕ, v_w, η are learning gains.

Ronsse et al. [26] showed that the traditional AO needs about 2 to 5 periods for convergence. Inevitably, an obvious phase error will be induced with a non-steady gait, such as switching from slow walking to rapid walking. To handle this problem, we use the difference between the right and left hip angle as input signals ($q = \theta_r - \theta_l$) so that it has a sine-like shape (see the shape of θ_r, θ_l, and q in Fig. 3). Moreover, we employ the zero-cross point ($q = 0, \dot{q} > 0$) to identify the zero phase and estimate the gait frequency by two adjacent zero phases with

$$\bar{w}(t) = \frac{2\pi}{T_k} = \frac{2\pi}{t_{z,k} - t_{z,k-1}} \tag{3}$$

where $\bar{w}(t)$ is the estimated frequency, $t_{z,k}$ and $t_{z,k-1}$ are the latest two adjacent zero-cross moments, and T_k is the period. We use the following new frequency update rule:

$$\dot{w}(t) = v_w \frac{e(t)}{\sum_{i=0}^{K} \alpha_i(t)} \cos\phi_1(t) + k_w \left(\bar{w}(t) - w(t)\right). \tag{4}$$

with

$$k_w = \begin{cases} \xi_w exp(-\frac{q^2}{2\sigma_w^2}) & 0 \le q \le d_w, \dot{q} > 0 \\ 0, \quad otherwise \end{cases} \tag{5}$$

where k_w is a nonlinear gain, ξ_w is the amplitude, σ_w is the bandwidth, d_w represents the correction region, q is the difference of two hip angles, and $\dot{q}$ is the derivative of q. A graphic illustration of k_w is shown in the blue region of Fig. 3. One can see that k_w has a maximum value at the zero-cross moment, then decreases rapidly. Compared with a fixed gain in [13], our proposed nonlinear gain is more reasonable

since the estimated frequency $\bar{w}(t)$ is accurate at the zero-cross point, and in general its authority decreases quickly when the point is far away from the zero-cross point. In this case, the oscillator dynamics is dominated by the conventional learning rules again (i.e., the white region in Fig. 3).

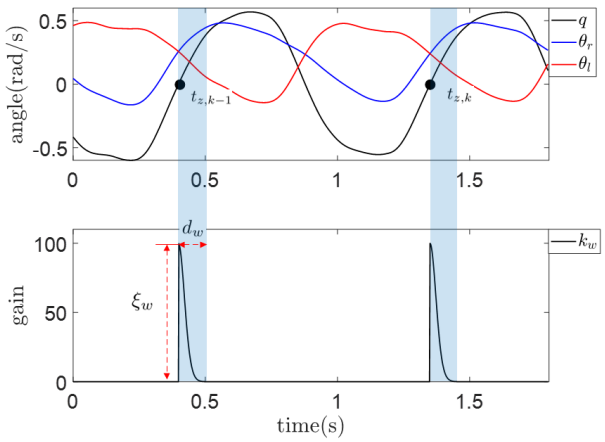

Fig. 3. A graphic illustration of k_w. The black solid dots represent the zero-cross point of q, θ_r and θ_l are the right hip angle and left hip angle, ξ_w represents the amplitude, and d_w represents the correction region.

In order to obtain a continuous gait phase between two adjacent zero-cross points, we integrate the gait frequency w and obtain the auxiliary phase as follows:

$$\phi_{aux} = \begin{cases} 0, t = t_{z,k} \\ \int w(t)dt, otherwise \end{cases} \tag{6}$$

where $t_{z,k}$ is the zero-cross moment. Note that ϕ_{aux} is different from the fundamental harmonic phase ϕ_1 since ϕ_{aux} resets at the zero-cross point. The auxiliary phase ϕ_{aux} is *not* involved in the oscillator dynamics so that it does not affect the oscillator stability. One remaining issue for (6) is that its end phase in a period may not be aligned to 2π. To alleviate this problem, we correct it as follows:

$$\phi_{aux,c} = \phi_{aux} + k_\phi(2\pi - \phi_{aux}) \tag{7}$$

with

$$k_\phi = \begin{cases} \xi_\phi exp(-\frac{q^2}{2\sigma_\phi^2}) & -d_\phi \le q \le 0, \dot{q} > 0 \\ 0, \quad otherwise \end{cases} \tag{8}$$

where ϕ_{aus} is the auxiliary phase, $\phi_{aux,c}$ is the corrected auxiliary phase, k_ϕ is a nonlinear gain, ξ_ϕ is the amplitude, d_ϕ is the correction window length, and σ_ϕ is the bandwidth. One can see that $\phi_{aux,c}$ is dominated by ϕ_{aus} when q is far away from the next zero-cross point, and is dominated by 2π when it approaches to the zero-cross point. Finally, the gait cycle can be estimated by

$$c = \frac{\text{mod}\ (\phi_{aux,c} - \pi/2, 2\pi)}{2\pi} \tag{9}$$

where $c \in [0, 1)$ is the gait cycle, mod is the modulo operation, and $\pi/2$ is an offset term (note that the zero phases correspond to the mid-swing phase, and $\pi/2$ is the estimated heel strike moment). Finally, the gait feature g can be obtained by

$$g = [w, \alpha_1, w\alpha_1]^T \tag{10}$$

where w is the estimated fundamental frequency, α_1 is the amplitude for the fundamental harmonic. A performance comparison of AO and RAO is shown in Section III-A.

In a practical application, it is necessary to classify walking and standing. This binary classifier is shown as follows:

$$\begin{cases} r = (q^2 + \gamma\dot{q}^2)^{0.5} > r_{start}, & walking \\ r = (q^2 + \gamma\dot{q}^2)^{0.5} < r_{stop}, & standing \end{cases} \tag{11}$$

where r is a distance metric, γ is a constant coefficient, r_{start} and r_{stop} are two thresholds. To avoid misclassification caused by disturbance, q and $\dot{q}$ are smoothed by a Butterworth filter. If the output of the classifier is walking, an assisted torque will be applied to the subject. Otherwise, the exoskeleton works at a zero torque mode.

C. Exoskeleton Controller

We use the pointwise minimum jerk curve [32] for the commanded torque generation. The torque is designed on the gait cycle and is shown in Fig. 4. Six variables control the shape of the profile. Among them, the offset and extension duration ext_{dur} are set to be user-specific but do *not* change with walking speed. Other parameters, i.e., the extension peak time ext_{peak}, the extension maximum torque ext_{max}, the flexion peak time fle_{peak} and flexion maximum torque fle_{max}, are speed-dependent and can be tuned in the training session.

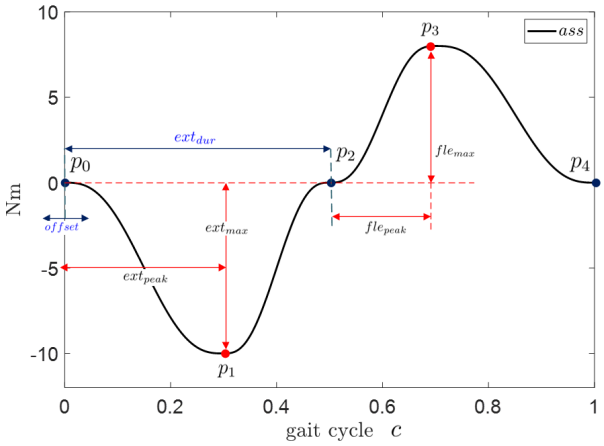

Fig. 4. Desired torque generator. The profile is controlled by both speed-independent parameters (offset time $offset$, extension duration ext_{dur}) and speed-dependent parameters (extension peak time ext_{peak}, extension maximum torque ext_{max}, flexion peak time fle_{peak}, and flexion maximum torque fle_{max}). The speed-independent parameters are determined before the training stage. At the training stage, users can select and submit their preferred speed-dependent parameters when walking at different speeds.

The torque controller is shown as

$$u = -\tilde{d} + k_p(\tau_d - \tau_a) + k_d\dot{\tau}_d \tag{12}$$

where $\tilde{d}$ is a nonlinear disturbance observer (NDOB) [33], τ_d is the desired torque, τ_a is the actual torque measured by torque sensor, k_p is a proportional term, and k_d is a feedforward term. The performance of the controller is shown in Section III-B.

D. Assistance Map Learning

The block diagram of this section is shown on the top of Fig. 2. It has two components: a training session and a learning session. In the training session, the exoskeleton is manipulated by the user who can adjust the assistance profile and submit their preferred parameters based on their proprioceptive feedback. Meanwhile, gait features g are extracted by RAO and paired with the preferred parameters. In the learning session, the GPR is utilized to construct assistance maps. After the learning session, the exoskeleton can automatically provide assistance without manipulating the human-robot interface.

The GPR's inputs are the gait features g extracted by RAO and the user selected parameter set Ψ. Its output is the predicted assistance parameter set $\bar{\Psi} = [\overline{ext}_{max}, \overline{ext}_{peak}, \overline{fle}_{max}, \overline{fle}_{peak}]^T$. We assume that the output elements are independent with each other. Then, we construct the parameter map for each element one by one. We use y to denote any output element. Then, we have

$$\begin{cases} f(g) = \Phi(g)^T \boldsymbol{w} \\ y = f(g) + \boldsymbol{\epsilon} \end{cases} \tag{13}$$

where $g \in \mathbb{R}^3$ is the gait feature vector, $f(g)$ maps g to a scalar, $\Phi(g)$ is a kernel function, $\boldsymbol{w}$ is the weight, and $\boldsymbol{\epsilon} \sim \mathcal{N}(0, \sigma^2 I)$ is the Gaussian noise with zero mean and covariance σ^2.

We denote the training set as $\mathcal{D} = \{(g_i, y_i)|i = 1, 2, \ldots, n\} = \{G, \boldsymbol{y}\}$ where $G \in \mathbb{R}^{3\times n}$ represents the input matrix, $\boldsymbol{y} \in \mathbb{R}^{n\times 1}$ represents target vector, and n is the number of samples. Then, the probability density of the observations given G and $\boldsymbol{w}$ can be shown as follows:

$$\begin{aligned} p(\boldsymbol{y}|G, \boldsymbol{w}) &= \Pi_{i=1}^n p(y_i|g_i, \boldsymbol{w}) \\ &= \Pi_{i=1}^n \frac{1}{\sqrt{2\pi}\sigma} \exp(-\frac{(y_i - \Phi(g_i)^T \boldsymbol{w})^2}{2\sigma^2}) \\ &= \frac{1}{(2\pi\sigma^2)^{1/2}} \exp(-\frac{1}{2\sigma^2} \left|\boldsymbol{y} - \Phi(G)^T \boldsymbol{w}\right|^2) \\ &\sim \mathcal{N}(\Phi(G)^T \boldsymbol{w}, \sigma^2 I_{n\times n}) \end{aligned} \tag{14}$$

where $\Phi(G)$ is the aggregation of columns $\Phi(g_i)$. Based on Bayes' rule, we have

$$p(\boldsymbol{w}|\boldsymbol{y}, G) = \frac{p(\boldsymbol{y}|G, \boldsymbol{w})p(\boldsymbol{w})}{p(\boldsymbol{y}|G)} \tag{15}$$

where the prior weight is assumed to be Gaussian with $\boldsymbol{w} \sim \mathcal{N}(0, \Sigma)$ (see equation (2.5) in [34]). Since the term $p(\boldsymbol{y}|G)$ is independent of $\boldsymbol{w}$, we have

$$\begin{aligned} &p(\boldsymbol{w}|\boldsymbol{y}, G) \propto p(\boldsymbol{y}|G, \boldsymbol{w})p(\boldsymbol{w}) \\ &\propto \exp(-\frac{1}{2\sigma^2}(\boldsymbol{y} - \Phi(G)^T \boldsymbol{w})^T (\boldsymbol{y} - \Phi(G)^T \boldsymbol{w})) \exp(-\frac{1}{2}\boldsymbol{w}^T \Sigma \boldsymbol{w}) \\ &\propto \exp(-\frac{1}{2}(\boldsymbol{w} - \bar{\boldsymbol{w}})^T (\frac{1}{\sigma_2}\Phi(G)\Phi(G)^T + \Sigma^{-1})(\boldsymbol{w} - \bar{\boldsymbol{w}})) \\ &\sim \mathcal{N}(\bar{\boldsymbol{w}}, A^{-1}) \end{aligned} \tag{16}$$

with

$$\begin{aligned} A &= \sigma^{-2}\Phi(G)\Phi(G)^T + \Sigma^{-1} \\ \bar{\boldsymbol{w}} &= \sigma^{-2} A^{-1} \Phi(G)\boldsymbol{y}. \end{aligned}$$

For a new input g_*, the predictive function $f_* \triangleq f(g_*)$ can be derived as an average over all possible weights. Thus, we have

$$\begin{aligned} p(f_*|g_*, G, \boldsymbol{y}) &= \int p(f_*|g_*, \boldsymbol{w})p(\boldsymbol{w}|G, \boldsymbol{y})d\boldsymbol{w} \\ &= \mathcal{N}(\sigma^{-2}\Phi(g_*)^T A^{-1}\Phi(G)\boldsymbol{y}, \Phi(g_*)^T A^{-1}\Phi(g_*)). \end{aligned} \tag{17}$$

To avoid the inversion of matrix A with size $n \times n$ which may be not convenient if n is large, equation (17) can be rewritten as

$$\begin{aligned} p(f_*|g_*, G, \boldsymbol{y}) =& \mathcal{N}(K_*^T (K + \sigma I)^{-1} \boldsymbol{y}, \\ & K_{**} - K_*^T (K + \sigma I)^{-1} K_*) \end{aligned} \tag{18}$$

where we define $K = \Phi^T \Sigma \Phi$, $K_* = \Phi^T \Sigma \Phi_*$, $K_{**} = \Phi_*^T \Sigma \Phi_*$, and $\Phi_* = \Phi(g_*)$, $\Phi = \Phi(G)$. Thus, we have

$$\begin{aligned} \bar{f}_* &= K_*^T (K + \sigma^2 I)^{-1} \boldsymbol{y} \\ V(f_*) &= K_{**} - K_*^T (K + \sigma^2 I)^{-1} K_* \end{aligned} \tag{19}$$

where $\bar{f}_*$ is the mean of f_* and $V(f_*)$ is the variance. More details can be found in [34, p.12].

The prediction probability in equation (18) is highly related to the covariance function. In this paper, we adopt the squared exponential covariance function as follows:

$$k(g_p, g_q) = \sigma_f^2 \exp(-\frac{1}{2}(g_p - g_q)^T \Sigma_l (g_p - g_q)) \tag{20}$$

where g_p, g_q are two input vectors, σ_f is the amplitude, Σ_l is a diagonal matrix. To optimize the hyperparameters $\boldsymbol{\theta} = (\sigma_f, \Sigma_l, \sigma)$, we calculate the log *marginal likelihood* as follows:

$$\begin{aligned} \log p(\boldsymbol{y}|G, \boldsymbol{\theta}) =& -\frac{1}{2}\boldsymbol{y}^T (K + \sigma^2 I)^{-1} \boldsymbol{y} \\ & - \frac{1}{2}\log|K + \sigma^2 I| - \frac{n}{2}\log 2\pi. \end{aligned} \tag{21}$$

Then, the optimal hyperparameters $\boldsymbol{\theta}$ can be obtained by solving the following equation:

$$\begin{aligned} \frac{\partial}{\partial \boldsymbol{\theta}_j}\log(\boldsymbol{y}|G, \boldsymbol{\theta}) &= \frac{1}{2}\boldsymbol{y}^T K^{-1}\frac{\partial K}{\partial \boldsymbol{\theta}_j}K^{-1}\boldsymbol{y} - \frac{1}{2}tr(K^{-1}\frac{\partial K}{\partial \boldsymbol{\theta}_j}) \\ &= 0 \end{aligned} \tag{22}$$

where $\theta_j \in \boldsymbol{\theta}$ is a parameter to be optimized (see [34, p.114]). Equation (22) can be solved by the modified conjugate gradient (CG) method [35]. After obtaining these hyperparameters, a predictive assistance parameter can be calculated based on (18) and the exoskeleton can automatically provide the assistance without manipulating the human-machine interface.

III. Experiments

A. Robust Adaptive Oscillators

To test the performance of RAO, a healthy subject (male, aged 28, weight 60 Kg, height 170 cm) walks on the ground with a hip exoskeleton in three modes: steady walking, speed up, and speed down. The input signal q is obtained by the difference of two hip encoders with $q = \theta_r - \theta_l$ and the tracking performance of RAO and AO is shown in Fig. 5. The real phase is obtained by offline linear interpolation while the zero phases are identified by the zero-cross point ($q = 0$, $\dot{q} > 0$). The real frequency is obtained by the reciprocal of time between two adjacent zero phases and is assumed to be

This article has been accepted for publication in IEEE Transactions on Medical Robotics and Bionics. This is the author's version which has not been fully edited and content may change prior to final publication. Citation information: DOI 10.1109/TMRB.2022.3206609

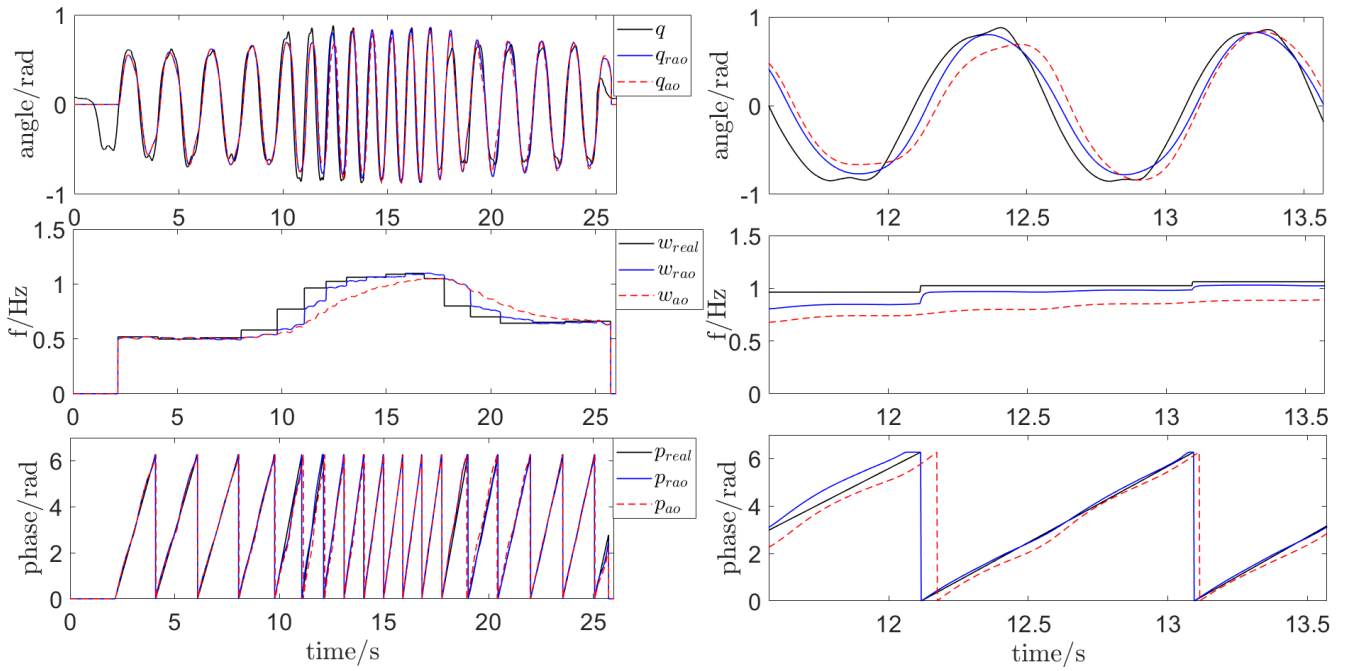

Fig. 5. Performance comparison of RAO and AO. The subject walks with a hip exoskeleton in three modes: steady walking, speed up, and speed down. RAO and AO have a similar performance with steady walking, while RAO's performance is better than AO with gait transition, such as speed up or speed down. The symbol q, w_{real}, p_{real} represents the input signal, the ground truth frequency, and the ground truth phase, respectively. The subscript rao and ao denotes the corresponding estimates using RAO and AO, respectively. A close-up with a speed-up gait is shown on the right. It can be seen that the frequency of RAO converges to the real frequency quickly at the zero-cross point. Moreover, its phase is aligned with the zero phases automatically.

constant among a stride. It can be seen that the performance of RAO and AO is similar in steady walking. However, the RAO has a faster convergence rate and owns a more accurate phase estimation in a non-steady gait. A close-up on the right of Fig. 5 supports this statement.

The error performance of RAO and AO is drawn in Fig. 6, in which we can see that the tracking error e_{qrao}, frequency error e_{wrao}, and phase error e_{prao} of RAO are smaller than that of values in AO. The RMSE metrics of these three indices are calculated and summarized in Table I. It can be seen that 20.46%, 36.82%, and 34.28% improvements are achieved by RAO compared with AO in terms of tracking error e_q, frequency error e_f, and phase error e_p.

TABLE I
PERFORMANCE COMPARISON OF RAO AND AO.

Items	RAO	AO	Reduction
RMSE of e_q (rad)	0.1245	0.1565	20.46%
RMSE of e_f (Hz)	0.0779	0.1232	36.82%
RMSE of e_p (rad)	0.1566	0.2383	34.28%

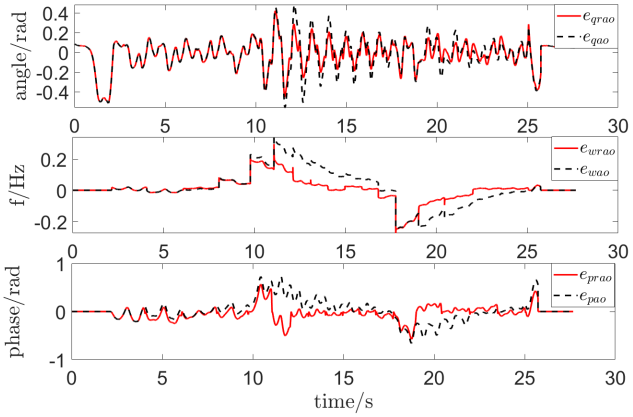

Fig. 6. Error performances of RAO and AO. The red lines represent the performance of RAO while the dashed black lines are errors of AO.

B. Torque Controller

As described in (12), the torque controller contains three parts: a NDOB term $\tilde{d}$, a proportional term $k_p(\tau_d - \tau_a)$ and a feedforward term $k_d\dot{\tau}_d$. To identify the influence of each term, three experiments are conducted. In the NDOB-KP-KD experiment, the torque controller is identical to (12). In the NDOB-KP experiment, the KD term is excluded. In the KP-KD experiment, the NDOB term is excluded. In all experiments, the desired torque is the same and the subject is required to walk on the treadmill at a speed of 3 km/h. The tracking performances of these three controllers are shown in Fig. 7. It can be seen that the first experiment performs the best while the third experiment is the worst. This indicates that the NDOB term can significantly improve the tracking performance. By comparing the results of the first experiment with the second experiment, we can see that the tracking delay can be compensated effectively by the feedforward term. Notably, in all experiments, there is an obvious tracking error around the heel strike moment. This is caused by the slack of the belt in the reducer (the reducer is composed of gear and belt).

This article has been accepted for publication in IEEE Transactions on Medical Robotics and Bionics. This is the author's version which has not been fully edited and content may change prior to final publication. Citation information: DOI 10.1109/TMRB.2022.3206609

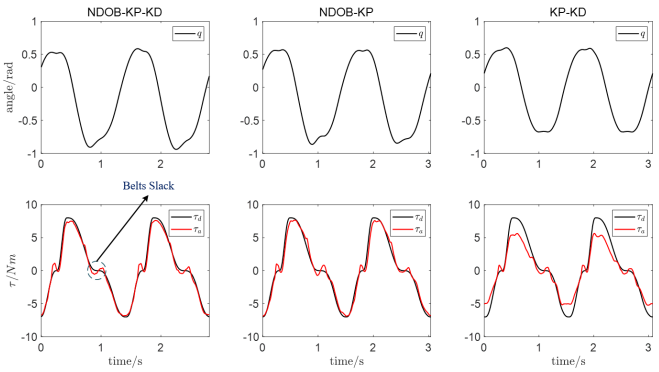

Fig. 7. Performance of three torque controllers. The signal q is shown on the top while the corresponding torque tracking performance is shown at the bottom.

Two metrics, the maximum error (ME) and the root mean squared error (RMSE), are calculated and summarized in Table II. It can be seen that the RMSE of the proposed controller is a mere 0.51 Nm, while it is 0.63 Nm and 1.42 Nm in the NDOB-KP controller and the KP-KD controller. As for the ME, it is 1.4 Nm in the original controller, while is as larger as 1.85 Nm and 2.83 Nm in the NDOB-KP controller and the KP-KD controller. These comparisons reveal that both the NDOB term and the feedforward term can improve the torque tracking performance effectively.

TABLE II
PERFORMANCE OF THE TORQUE CONTROLLER.

Controller	ME (Nm)	RMSE (Nm)
NDOB-KP-KD	1.40	0.51
NDOB-KP	1.85	0.63
KP-KD	2.83	1.42

C. Parameters Map Learning

Seven subjects (aged 28.1 ± 4.1; weight 65.9 ± 10.9 kg; height 171.6 ± 3.5 cm; mean $\pm$ S.D.) participate in the experiment. The experiment contains two sessions: a warm-up session and a test session. The warm-up session is arranged on the first day and participants are guided on how to manipulate the exoskeleton. In this session, participants are required to select the offset variable $offset$ and extension duration variable ext_{dur} so that the extension torque appears at the heel strike moment and flexion torque appears at the toe-off moment. The test session is conducted on the following day. In this session, subjects are required to walk on the treadmill with a hip exoskeleton from a speed of 1.5 km/h to 5.0 km/h with an increment of 0.5 km/h and select their preferred parameters ext_{max}, ext_{peak}, fle_{max} and fle_{peak}. At each speed, three gaits are required to be involved which include a natural gait, a small amplitude gait, and a big amplitude gait. Subjects can adjust the assistance profile by an interactive screen and submit their preferred parameters according to the following criteria: the exoskeleton can reduce their biological effort effectively; the interaction force is comfortable. The experimental setup and the interactive screen are shown in Fig. 8. Notably, subjects can submit either one group of parameters or multiple groups of parameters under each gait. These parameters, together with the gait features, will be used for assistance map learning.

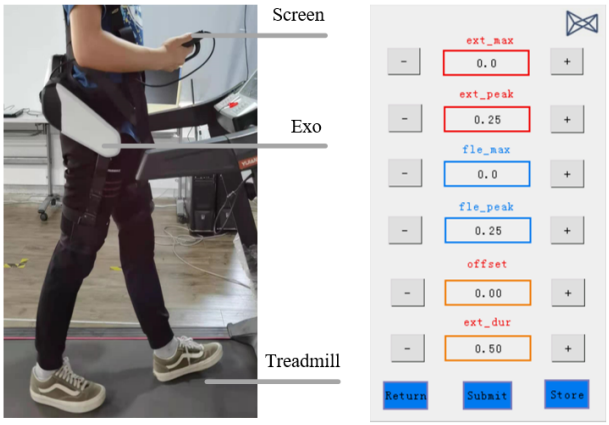

Fig. 8. Experimental setup and the interactive screen. Six parameters are contained in the screen which corresponds to Fig. 4. Among them, offset $offset$ and extension duration ext_{dur} are determined in the warm-up session and remain unchanged in the following session, while the other parameters (ext_{max}, ext_{peak}, fle_{max}, fle_{peak}) are tuned in the test session.

The assistance map is constructed using equations (13)-(22) in MATLAB offline. After the learning procedure, the learned assistance maps are downloaded to the microprocessor of the hip exoskeleton. Then, the exoskeleton can provide individualized assistance when walking under different gaits without manipulating the interface. The maps of ext_{max}, ext_{peak}, fle_{max}, fle_{peak} for three subjects (S1, S2 and S3) are drawn in Fig. 9. The assistance maps for the other four participants are shown in Figs. 3 and 4 of the supplementary material. From these figures, one can see that there is a substantial parameter difference among subjects, which indicates that one subject's preferred assistance profile may be disfavored by another. Generally, the values of ext_{max} and fle_{max} increase with the growth of frequency w and amplitude α, although fluctuation and owing a different ratio. As for ext_{peak} and fle_{peak}, they are much more irregular and different from person to person. A common characteristic of ext_{peak} and fle_{peak} is that these points are statistically located around the midpoint of extension duration and flexion duration, revealing that subjects dislike a sharp assistance transition.

It is worth noting that the learning efficiency of the proposed method improves significantly compared with the traditional HIL optimization. In our experiment, participants spend 20.1 ± 2.5 minutes to learn a total of 24 kinds of gaits, which is significantly less than 83 ± 14 and 21.4 ± 1 minutes for a single gait in [1] and [2], respectively (see Table. III). In addition, our proposed method does not require specific instruments, and the training procedure can be conducted at any place (the training process does not strictly require a treadmill). Hence, it is more convenient and efficient compared with HIL optimization.

This article has been accepted for publication in IEEE Transactions on Medical Robotics and Bionics. This is the author's version which has not been fully edited and content may change prior to final publication. Citation information: DOI 10.1109/TMRB.2022.3206609

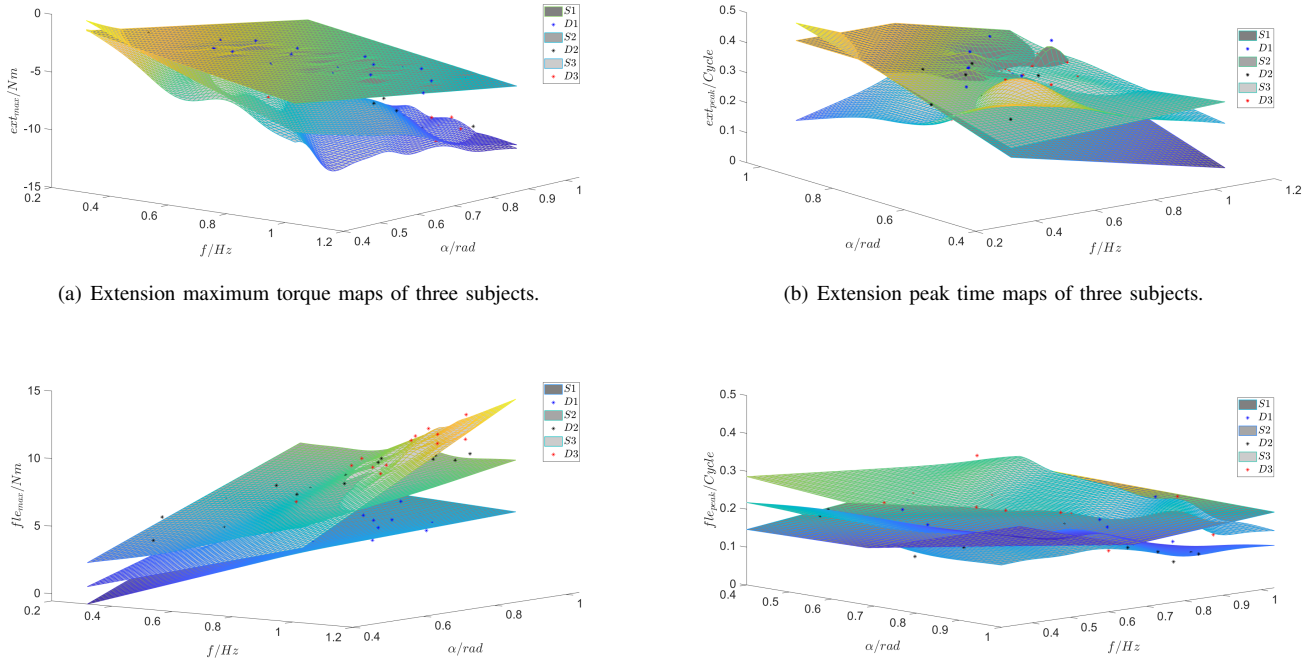

(a) Extension maximum torque maps of three subjects.

(b) Extension peak time maps of three subjects.

(c) Flexion maximum torque maps of three subjects.

(d) Flexion peak time maps of three subjects.

Fig. 9. The learned assistance maps. The star $*$ represents the user-selected parameters, the predicted values is drawn by mesh figures.

TABLE III
LEARNING EFFICIENCY COMPARISON OF DIFFERENT METHODS.

Methods	Parameters	Gaits	Time Cost
CMA-ES [1]	4	1	83 ± 14 min
Bayesian Optimization [2]	2	1	21.4 ± 1 min
Body-in-the-loop [24]	1	1	50 min
Proposed Method	4	24	20.1 ± 2.5 min

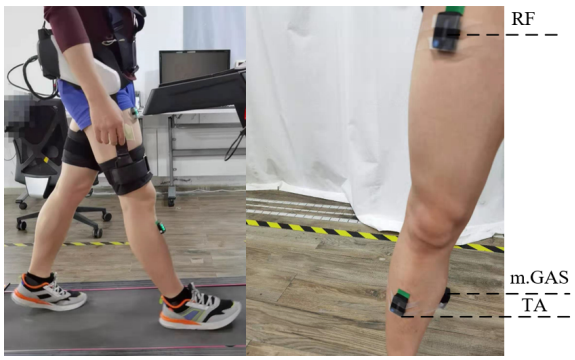

Fig. 10. Experimental scenario and sEMG sensor placement. Three muscles are involved in this experiment, which are RF, TA, and m.GAS. The desired torque is generated based on the user's preference.

D. Investigation of Muscle Activities

To investigate the performance of the user-preferred assistance profile, an experiment is conducted with sEMG sensors (Trigno, Delsys, USA). Three muscles are considered in this experiment, which include rectus femoris (RF), tibialis anterior (TA), and medial gastrocnemius (m.GAS). Seven participants participate in the experiments and the desired torque is obtained based on the user's preference. The experimental scenario and the sensor placement are shown in Fig.10.

The experiment is approved by the Ethics Committee of HKUST. Subjects are asked to walk on the treadmill at a speed of 5 km/h in three conditions: zero torque (ZT), assistance (ASS), and normal walking (NW). Each condition lasts 2 minutes to achieve a steady gait and an additional 2 minutes break is given between two modes to avoid fatigue. The sampling frequency of sEMG sensors is 2148 Hz. The raw data is first butter filtered, then offset removed. The sEMG envelope is obtained by its root mean square (RMS) values and the corresponding window length is 0.125 s. The orientation of the thigh and shank is obtained by inertial measurement units (IMUs) that integrated into the sEMG sensor. The gait cycle is segmented by the maximum hip angle obtained by IMUs and the sEMG envelope is averaged and normalized to a stride. We use the last-minute data of each walking condition for calculation.

The user-preferred torque and the actual torque measured by a torque sensor are shown in Fig. 5 of the supplementary material. The envelope muscle activities of seven subjects in different conditions are shown in Fig. 11. The sEMG amplitudes are normalized to the averaged peak values of the data in the NW condition. It can be seen that there is an obvious muscle activity reduction in the ASS mode compared with ZT mode, which indicates that the user-selected assistance profile can reduce the biological efforts.

We use the RMS sEMG envelope values over a stride for

This article has been accepted for publication in IEEE Transactions on Medical Robotics and Bionics. This is the author's version which has not been fully edited and content may change prior to final publication. Citation information: DOI 10.1109/TMRB.2022.3206609

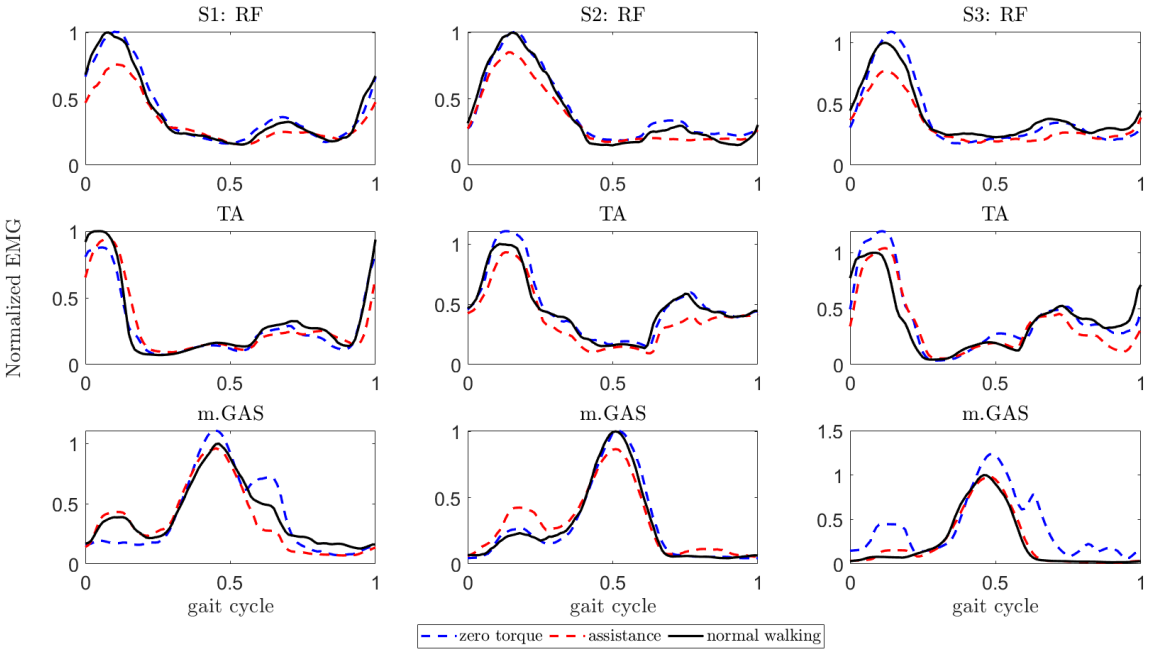

(a) sEMG signals of S1, S2, and S3.

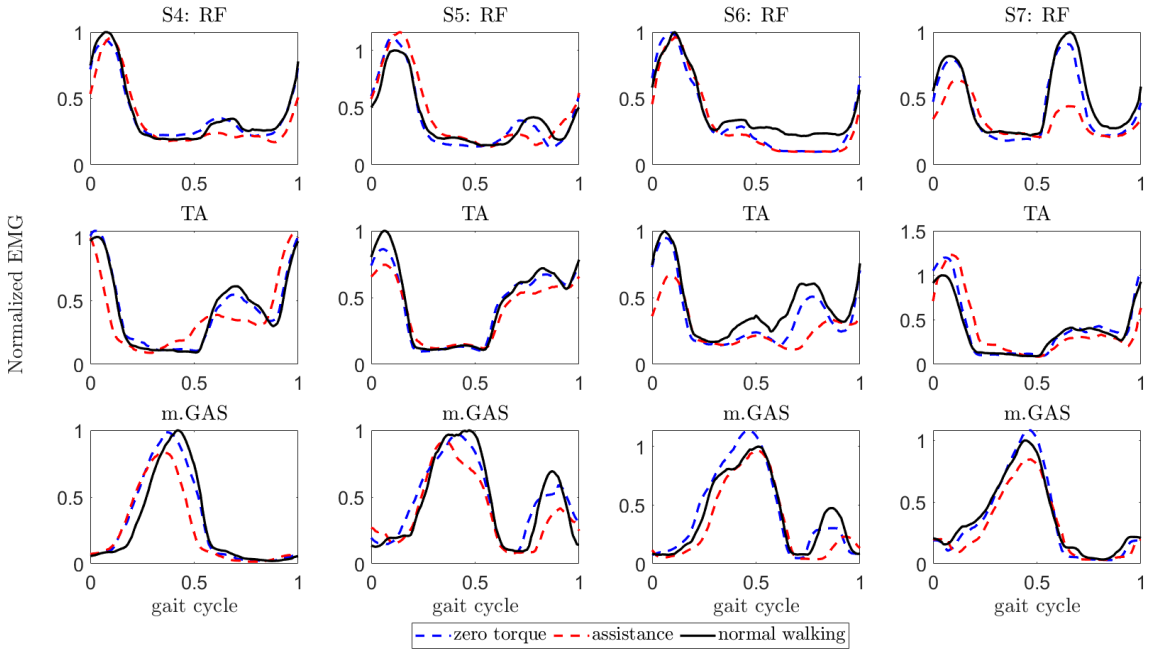

(b) sEMG signals of S4, S5, S6, and S7.

Fig. 11. Muscle activities of seven subjects in three conditions: ZT, ASS, and NW. The envelopes are normalized to the values in the NW condition.

the comparison of muscle activities among different walking modes. It can be seen that all muscle activities are reduced in the ASS mode compared to ZT mode or NW mode (see Fig. 12). Meanwhile, m.GAS has a statistically significant difference in the ASS compared with ZT and NW, and the corresponding reductions are $15.63 \pm 6.51\%$ and $8.73 \pm 6.4\%$, respectively. The detailed comparison is summarized in Table IV where the superscript $*$ denotes statistically significant differences with respect to ZT, while $**$ denotes statistically significant differences with respect to NW ($p < 0.05$).

TABLE IV
MUSCLE ACTIVITY COMPARISON.

Muscle	ASS-ZT(mean $\pm$ S.D.%)	ASS-NW(mean $\pm$ S.D.%)
RF	$-12.70 \pm 12.59^{*}$	-13.49 ± 14.85
TA	$-11.40 \pm 10.16^{*}$	-11.24 ± 14.43
m.GAS	$-15.63 \pm 6.51^{*}$	$-8.73 \pm 6.40^{**}$

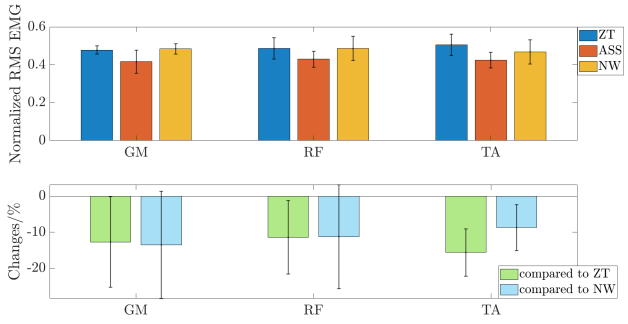

Fig. 12. Normalized muscle activities and their changes in the assistance mode compared to ZT mode and NW mode.

IV. Conclusion

In the paper, we present a RAO for human-robot synchronization, which has a faster convergence rate and smaller phase error compared with the conventional AO. Moreover, we develop a GPR strategy for assistance map construction, which is both convenient and efficient. Experiments are conducted to verify the performance of the user-selected profile. Results show that the user-selected assistance can achieve a biological effort reduction compared with the zero torque mode and normal walking.

Our experiment also implies that the user-preferred assistance map is highly personalized and is different from person to person. This indicates that unified assistance is not feasible for users since the preferred assistance for one person may be disfavored by another. Our work provides a possible solution to integrate the user's preference into the exoskeleton control and presents an assistance map construction approach for walking assistance in a community.

References

[1] J. Zhang, P. Fiers, K. A. Witte, R. W. Jackson, K. L. Poggensee, C. G. Atkeson, and S. H. Collins, "Human-in-the-loop optimization of exoskeleton assistance during walking," *Science*, vol. 356, no. 6344, pp. 1280–1284, 2017.

[2] Y. Ding, M. Kim, S. Kuindersma, and C. J. Walsh, "Human-in-the-loop optimization of hip assistance with a soft exosuit during walking," *Science Robotics*, vol. 3, no. 15, 2018.

[3] W. Wang, J. Chen, Y. Ji, W. Jin, J. Liu, and J. Zhang, "Evaluation of lower leg muscle activities during human walking assisted by an ankle exoskeleton," *IEEE Transactions on Industrial Informatics*, vol. 16, no. 11, pp. 7168–7176, 2020.

[4] S. H. Collins, M. B. Wiggin, and G. Sawicki, "Reducing the energy cost of human walking using an unpowered exoskeleton," *Nature*, vol. 522, pp. 212 – 215, 2015.

[5] R. Nasiri, A. Ahmadi, and M. N. Ahmadabadi, "Reducing the energy cost of human running using an unpowered exoskeleton," *IEEE Transactions on Neural Systems and Rehabilitation Engineering*, vol. 26, no. 10, pp. 2026–2032, Oct 2018.

[6] L. N. Awad, J. Bae, K. O'Donnell, S. M. M. De Rossi, K. Hendron, L. H. Sloot, P. Kudzia, S. Allen, K. G. Holt, T. D. Ellis, and C. J. Walsh, "A soft robotic exosuit improves walking in patients after stroke," *Science Translational Medicine*, vol. 9, no. 400, 2017.

[7] J. Bae, C. Siviy, M. Rouleau, N. Menard, K. O'Donnell, I. Geliana, M. Athanassiu, D. Ryan, C. Bibeau, L. Sloot, P. Kudzia, T. Ellis, L. Awad, and C. J. Walsh, "A lightweight and efficient portable soft exosuit for paretic ankle assistance in walking after stroke," in *2018 IEEE International Conference on Robotics and Automation (ICRA)*, 2018, pp. 2820–2827.

[8] J. Kim, G. Lee, R. Heimgartner, D. Arumukhom Revi, N. Karavas, D. Nathanson, I. Galiana, A. Eckert-Erdheim, P. Murphy, D. Perry, N. Menard, D. K. Choe, P. Malcolm, and C. J. Walsh, "Reducing the metabolic rate of walking and running with a versatile, portable exosuit," *Science*, vol. 365, no. 6454, pp. 668–672, 2019.

[9] J. Yang, T.-H. Huang, S. Yu, X. Yang, H. Su, A. M. Spungen, and C.-Y. Tsai, "Machine learning based adaptive gait phase estimation using inertial measurement sensors," in *Frontiers in Biomedical Devices*, vol. 41037. American Society of Mechanical Engineers, 2019, p. V001T09A010.

[10] R. Ronsse, N. Vitiello, T. Lenzi, J. van den Kieboom, M. C. Carrozza, and A. J. Ijspeert, "Human-robot synchrony: Flexible assistance using adaptive oscillators," *IEEE Transactions on Biomedical Engineering*, vol. 58, no. 4, pp. 1001–1012, 2011.

[11] Keehong Seo, SeungYong Hyung, Byung Kwon Choi, Younbaek Lee, and Youngbo Shim, "A new adaptive frequency oscillator for gait assistance," in *2015 IEEE International Conference on Robotics and Automation (ICRA)*, 2015, pp. 5565–5571.

[12] E. Zheng, S. Manca, T. Yan, A. Parri, N. Vitiello, and Q. Wang, "Gait phase estimation based on noncontact capacitive sensing and adaptive oscillators," *IEEE Transactions on Biomedical Engineering*, vol. 64, no. 10, pp. 2419–2430, 2017.

[13] K. Seo, K. Kim, Y. J. Park, J. Cho, J. Lee, B. Choi, B. Lim, Y. Lee, and Y. Shim, "Adaptive oscillator-based control for active lower-limb exoskeleton and its metabolic impact," in *2018 IEEE International Conference on Robotics and Automation (ICRA)*, 2018, pp. 6752–6758.

[14] T. O. M. Tao Xue, Ziwei Wang and Bin Han, "A new delayless adaptive oscillator for gait assistance," in *2020 IEEE/RSJ International Conference on Intelligent Robots and Systems (IROS)*, 2020, pp. 3459–3464.

[15] C. Lovejoy, "The natural history of human gait and posture: Part 1. spine and pelvis," *Gait Posture*, vol. 21, no. 1, pp. 95 – 112, 2005.

[16] V. Dietz, "Spinal cord pattern generators for locomotion," *Clinical Neurophysiology*, vol. 114, no. 8, pp. 1379 – 1389, 2003.

[17] M. Kim and S. H. Collins, "Once-per-step control of ankle push-off work improves balance in a three-dimensional simulation of bipedal walking," *IEEE Transactions on Robotics*, vol. 33, no. 2, pp. 406–418, 2017.

[18] G. Lee, J. Kim, F. A. Panizzolo, Y. M. Zhou, L. M. Baker, I. Galiana, P. Malcolm, and C. J. Walsh, "Reducing the metabolic cost of running with a tethered soft exosuit," *Science Robotics*, vol. 2, no. 6, 2017.

[19] S. H. Collins and A. D. Kuo, "Recycling energy to restore impaired ankle function during human walking," *PLoS one*, vol. 5, no. 2, p. e9307, 2010.

[20] K. E. Zelik, S. H. Collins, P. G. Adamczyk, A. D. Segal, G. K. Klute, D. C. Morgenroth, M. E. Hahn, M. S. Orendurff, J. M. Czerniecki, and A. D. Kuo, "Systematic variation of prosthetic foot spring affects center-of-mass mechanics and metabolic cost during walking," *IEEE Transactions on Neural Systems and Rehabilitation Engineering*, vol. 19, no. 4, pp. 411–419, 2011.

[21] B. T. Quinlivan, S. Lee, P. Malcolm, D. M. Rossi, M. Grimmer, C. Siviy, N. Karavas, D. Wagner, A. Asbeck, I. Galiana, and C. J. Walsh, "Assistance magnitude versus metabolic cost reductions for a tethered multiarticular soft exosuit," *Science Robotics*, vol. 2, no. 2, 2017.

[22] A. J. Young, J. Foss, H. Gannon, and D. P. Ferris, "Influence of power delivery timing on the energetics and biomechanics of humans wearing a hip exoskeleton," *Frontiers in Bioengineering and Biotechnology*, vol. 5, no. 4, 2017.

[23] J. Lee, K. Seo, B. Lim, J. Jang, K. Kim, and H. Choi, "Effects of assistance timing on metabolic cost, assistance power, and gait parameters for a hip-type exoskeleton," in *2017 International Conference on Rehabilitation Robotics (ICORR)*, 2017, pp. 498–504.

[24] J. Koller, D. Gates, D. P. Ferris, and C. D. Remy, "Body-in-the-loop optimization of assistive robotic devices: A validation study," in *Robotics: Science and Systems*, 2016.

[25] Ludovic Righetti, Jonas Buchli, and Auke Jan Ijspeert, "Dynamic hebbian learning in adaptive frequency oscillators," *Physica D: Nonlinear Phenomena*, vol. 216, no. 2, pp. 269 – 281, 2006.

[26] R. Ronsse, S. M. M. De Rossi, N. Vitiello, T. Lenzi, M. C. Carrozza, and A. J. Ijspeert, "Real-time estimate of velocity and acceleration of quasi-periodic signals using adaptive oscillators," *IEEE Transactions on Robotics*, vol. 29, no. 3, pp. 783–791, 2013.

[27] P. R. Davidson and D. M. Wolpert, "Widespread access to predictive models in the motor system: a short review," *Journal of Neural Engineering*, vol. 2, no. 3, pp. S313–S319, aug 2005.

[28] C. Basu, Q. Yang, D. Hungerman, M. Sinahal, and A. D. Draqan, "Do you want your autonomous car to drive like you?" in *2017 12th*

ACM/IEEE International Conference on Human-Robot Interaction (HRI, 2017, pp. 417–425.

[29] O. Chapelle, T. Joachims, F. Radlinski, and Y. Yue, "Large-scale validation and analysis of interleaved search evaluation," *ACM Trans. Inf. Syst.*, vol. 30, no. 1, mar 2012.

[30] M. Tucker, E. Novoseller, C. Kann, Y. Sui, Y. Yue, J. W. Burdick, and A. D. Ames, "Preference-based learning for exoskeleton gait optimization," in *2020 IEEE International Conference on Robotics and Automation (ICRA)*, 2020, pp. 2351–2357.

[31] J. E. A. Bertram, "Constrained optimization in human walking: cost minimization and gait plasticity," *Journal of Experimental Biology*, vol. 208, no. 6, pp. 979–991, 2005.

[32] A. Piazzi and A. Visioli, "Global minimum-jerk trajectory planning of robot manipulators," *IEEE Transactions on Industrial Electronics*, vol. 47, no. 1, pp. 140–149, 2000.

[33] Wen-Hua Chen, D. J. Ballance, P. J. Gawthrop, and J. O'Reilly, "A nonlinear disturbance observer for robotic manipulators," *IEEE Transactions on Industrial Electronics*, vol. 47, no. 4, pp. 932–938, 2000.

[34] C. E. Rasmussen and C. K. I. Williams, *Gaussian Processes for Machine Learning (Adaptive Computation and Machine Learning)*. The MIT Press, 2005.

[35] T. Steihaug, "The conjugate gradient method and trust regions in large scale optimization," *SIAM Journal on Numerical Analysis*, vol. 20, no. 3, pp. 626–637, 1983.